

**Structure-based de novo design and identification of D816V
mutant-selective c-KIT inhibitors**

Journal:	<i>Organic & Biomolecular Chemistry</i>
Manuscript ID:	OB-ART-01-2014-000053.R1
Article Type:	Paper
Date Submitted by the Author:	29-Jan-2014
Complete List of Authors:	Park, H; Sejong University, Lee, Soyoung; KAIST, Lee, Suhyun; KAIST, Hong, Sungwoo; KAIST, Chemistry

Cite this: DOI: 10.1039/c0xx00000x

www.rsc.org/xxxxxx

ARTICLE TYPE

Structure-based *de novo* design and identification of D816V mutant-selective c-KIT inhibitors

Hwangseo Park,^{*a} Soyoung Lee,^b Suhyun Lee,^b and Sungwoo Hong^{*b}

Received (in XXX, XXX) Xth XXXXXXXXX 20XX, Accepted Xth XXXXXXXXX 20XX

DOI: 10.1039/b000000x

To identify potent and selective inhibitors of D816V, the most common gain-of-function c-KIT mutant, we carried out structure-based *de novo* design using 7-azaindole as the core and the scoring function improved by implementing an accurate solvation free energy term. This approach led to the identification of new c-KIT inhibitors specific for the D816V mutant. The 3-(3,4-dimethoxyphenyl)-7-azaindole scaffold was optimized and represents a lead structure for the design of the potent and specific inhibitors of the D816V mutant. The results of molecular dynamics simulations indicate that hydrogen bond interactions between the 7-azaindole moiety and the backbone groups of Cys673 are the most significant determinant for the potency and selectivity of c-KIT inhibitors.

Introduction

The stem cell factor receptor (c-KIT) is a receptor tyrosine kinase that is activated through dimerization upon binding stem cell factor (SCF). Activated c-KIT phosphorylates intracellular substrates and thereby switches on downstream cell signaling pathways essential for cell proliferation, differentiation, and survival.¹ Deregulated c-KIT kinase activity is responsible for the pathogenesis of various human cancers, including acute myeloid leukemia, small cell lung carcinoma, malignant melanomas, colorectal cancer, and gastrointestinal stromal tumors.²

Most cancers caused by c-KIT abnormalities stem from a subset of mutations that render c-KIT kinase constitutively active.³ The activation loop (A-loop) of the wild-type c-KIT exists in dynamic equilibrium between the active and inactive conformations. Mutations that induce tumorigenic effects have been identified in a membrane-proximal immunoglobulin-like domain, the auto-inhibitory juxtamembrane region (JMR), and the protein tyrosine kinase domain.⁴ The mutation of Asp816 in the A-loop to Val is the most frequently observed c-KIT mutation in human cancers.⁵ This D816V mutant of c-KIT is capable of inducing downstream oncogenic signaling regardless of ligand binding in the extracellular region.⁶ With respect to this unusual activation, recent molecular dynamics (MD) simulation studies have shown that the activating D816V mutation promotes spontaneous detachment of the JMR from the kinase domain, which is the triggering first step of the inactive-to-active state transition of c-KIT.⁷ Imatinib is effective against wild-type c-KIT by stabilizing the inactive conformation of the kinase domain, but introduction of the D816V point mutation disrupts the inactive

conformation. Because the active conformation of the c-KIT kinase domain is strongly favored in D816V mutant through ligand independent constitutive auto phosphorylation, the D816V mutant is resistant to imatinib which targets the inactive conformation of c-KIT.⁸ The emergence of c-KIT mutants that are resistant to first-line drugs has complicated clinical treatment, highlighting the importance of identifying new c-KIT inhibitors with high potency against D816V mutant for use as second-line treatments.

Although the importance of constitutively active c-KIT mutants in the pathogenesis of human cancers is well appreciated, the discovery of inhibitors specific for such gain-of-function mutants lags behind biochemical and pharmaceutical studies. A few compounds, such as AP23464 and AP23848 with a modest degree of selectivity (~10-fold) toward D816V relative to wild-type c-KIT have been described.⁹ The basis of selectivity in this case could be attributed to the decrease in binding affinity for the inactive conformation of wild-type c-KIT. Because the normal activity of wild-type c-KIT is necessary for the survival, differentiation, and function of mast cells, the selective inhibition of c-KIT gain-of-function mutants with small-molecule inhibitors can be a novel strategy for the development of anticancer agents that do not disrupt normal SCF/KIT signaling, thereby minimizing the risk of potential toxicity.

In this study, we seek to identify potent and selective inhibitors for the most abundant gain-of-function c-KIT mutant (D816V) based on the structure-based *de novo* design, chemical synthesis, and biochemical evaluation of various derivatives of 7-azaindole. Because this chemical scaffold binds tightly at the hinge region (Cys673), it is predicted to serve as a good starting point from which potent and selective inhibitors can be derived.¹⁰ To improve correlation between computational predictions and experimentally obtained biological data, we used an accurate solvation model for calculating the binding free energies between c-KIT and putative ligands (See the Supporting Information for more details).¹¹ By applying MD simulations of wild-type c-KIT and the D816V mutant in complex with the newly identified inhibitors, we also address the structural and dynamic features for the design of potent and selective inhibitors of the D816V mutant.

Results and discussion

Because no X-ray crystal structure of the D816V mutant was available, its atomic coordinates were obtained by homology

modeling using the structure of wild-type c-KIT in the active conformation as the template (PDB entry: 1PKG).¹² In this structure, the JMR and A-loop were in open positions to allow free access of bulk solvent to the active site. Homology modeling of D816V mutant of c-KIT constructed by MODELLER program¹³ was useful because the coordinates of missing residues (residues 694–762) in the original X-ray structure of the template could be built in the target from a randomized distorted structure that resides approximately between the two anchoring regions. The calculated structure of D816V mutant appeared to be quite similar to that of wild-type in the active conformation.¹⁴ As the receptor model for wild-type c-KIT to be used in structure-based design, we utilized the X-ray crystal structure of c-KIT in the autoinhibited conformation (PDB entry: 1T45).¹⁵ The JMR segment was entered into the active site in this inactive conformation, which led to the obstruction of the active site by the A-loop.¹⁶ Using these two receptor models—the D816V mutant and the autoinhibited wild-type c-KIT—we perform *de novo* design of 7-azaindole derivatives to identify potent and selective inhibitors of the gain-of-function mutant.¹⁷

To obtain the starting structure for *de novo* design, we carried out docking simulations of 7-azaindole in the ATP-binding site of c-KIT. The binding modes of 7-azaindole for wild-type c-KIT and the D816V mutant were obtained with the modified scoring function and compared in Figure 1. In both structures, 7-azaindole appears to be stabilized through bidentate hydrogen bonds with the backbone amide group of Cys673 in the hinge region and hydrophobic interactions with the side chain of Tyr672 in the ATP-binding site. Despite the similarity in the interactions of 7-azaindole in the wild-type c-KIT and the D816V mutant, 7-azaindole derivatives with large substituents are expected to have different binding modes owing to the differences in the configuration of key structural elements between the wild-type and mutant c-KIT. For example, the glycine-rich phosphate-binding loop (P-loop) stays quite distant from 7-azaindole and points to the solvent area in wild-type c-KIT (Figure 2a), whereas it forms a binding pocket in the D816V mutant (Figure 2b). In the calculated binding modes shown in Figure 2, we also note that the 6-membered ring of 7-azaindole stays closer to the P-loop than the 5-membered ring. Therefore, the introduction of a substituent at the pyridine ring of 7-azaindole seems to increase the potency for the D816V mutant only without significantly changing the inhibitory activity against wild-type c-KIT. Actually, we have been able to identify selective and potent inhibitors of D816V mutant via *de novo* design of 7-azaindole derivatives based on the differences in calculated structures of c-KIT-azaindole and D816V-azaindole complexes.

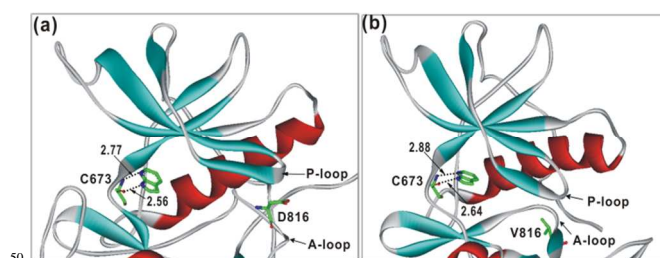
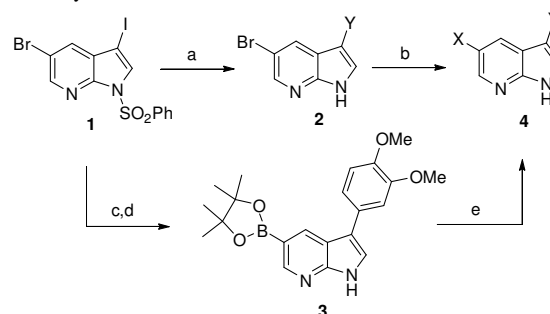


Figure 1 Docking poses of 7-azaindole in the ATP-binding sites of (a) wild-type c-KIT in the inactive conformation and (b) the active form of D816V mutant. X-ray structure of the wild type (a) and the homology-modeled structure of D816V mutant (b) were used in the calculations. Each dotted line indicates a hydrogen bond.

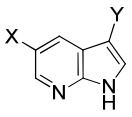
Next, structure-based *de novo* design of new c-KIT inhibitors specific for the D816V mutant was conducted, and a variety of drug-like 7-azaindole derivatives were generated with the LigBuilder program (Figure S1 in the Supporting Information for more details).¹⁸ The generated 7-azaindole derivatives were then scored according to the calculated binding free energy with respect to the D816V mutant. The synthetic approach to the 7-azaindole analogs is shown in Scheme 1.¹⁹ First, Pd-catalyzed coupling was conducted at 80 °C with the C5 (hetero) aryl partners for functionalization of the C3 position. The benzenesulfonyl group was removed under the basic reaction conditions to provide intermediate **2**. An assortment of C5 functional groups was then explored by subjecting compound **2** to another Pd-catalyzed Suzuki coupling with the appropriate boronic acids or boronic esters at 100 °C. The enhanced potency produced by introduction of the 3, 4-dimethoxyphenyl group at the C3 position of 7-azaindole suggested a broader exploration of derivatives that incorporated this key functional group (Table 1). In this regards the synthesis of 3-(3,4-dimethoxyphenyl)-7-azaindole derivatives, was facilitated by converting 5-bromoazaindole into the corresponding boronic esters **3** via direct borylation reaction. Various (hetero)aryl groups were then installed to the 5-position using Suzuki coupling with the appropriate (hetero)aryl boronic acid. In the final step, IC₅₀ (50% inhibitory concentration) values for the synthesized derivatives were then determined against both the wild-type c-KIT and D816V mutant.²⁰

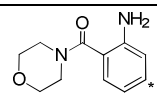
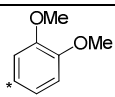
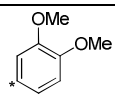
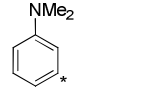
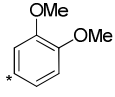
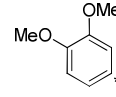
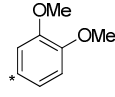
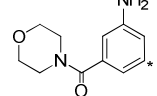
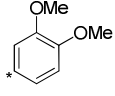
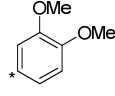
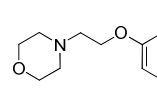
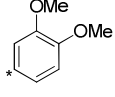
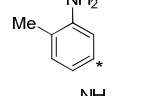
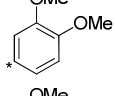
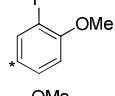
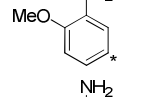
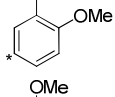
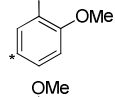
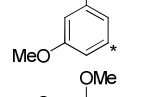
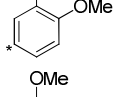
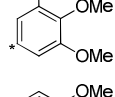
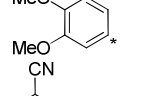
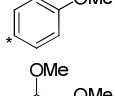
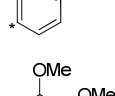
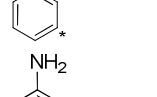
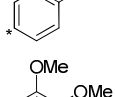
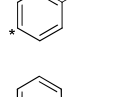
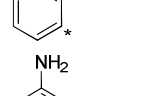
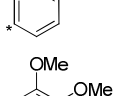
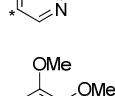
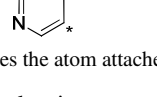
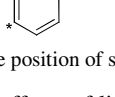
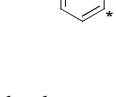
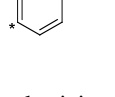
Scheme 1 Synthetic route of azaindole derivatives.^a



^a Reagents and conditions: (a) aryl boronic acid, Pd(dppf)Cl₂·CH₂Cl₂, Cs₂CO₃, 1,4-dioxane:H₂O = 3:1, 80 °C, 2 h, then 4N KOH, MeOH, 60 °C, 1 h; (b) aryl boronic acid, Pd(dppf)Cl₂·CH₂Cl₂, Cs₂CO₃, 1,4-dioxane:H₂O = 3:1, 100 °C, 4 h; (c) 3,4-dimethoxyphenylboronic acid, Pd(dppf)Cl₂·CH₂Cl₂, Cs₂CO₃, 1,4-dioxane:H₂O = 3:1, 80 °C, 2 h, then 4N KOH, 60 °C, 1 h; (d) bis(pinicolato)diboron, Pd(dppf)Cl₂·CH₂Cl₂, KOAc, 1,4-dioxane, 90 °C, 12 h; (e) aryl bromide, Pd(dppf)Cl₂·CH₂Cl₂, Cs₂CO₃, 1,4-dioxane:H₂O = 3:1, 100 °C, 4 h.

Table 1 lists the structures and IC₅₀ values of 22 representative inhibitors. We note that most 7-azaindole derivatives exhibit a higher potency against the D816V mutant than wild-type c-KIT. Because all 7-azaindole derivatives were selected to maximize the affinity for the D816V mutant and minimize the affinity for wild-type c-KIT, the potency and selectivity of the designed inhibitors exemplify the accuracy of the modified scoring

Table 1 Structures and Inhibitory Activities of Representative 7-Azaindole Derivatives.


	X ^a	Y ^a	IC ₅₀ (nM) for KIT		X ^a	Y ^a	IC ₅₀ (nM) for KIT		
			WT	D816V			WT	D816V	
5			9140	8.5	16			>10000	261.4
6			>10000	29.2	17			142.0	2.1
7			>10000	15.8	18			3327	60.1
8			8540	13.9	19			1743	47.8
9			>10000	24.6	20			1822	104.1
10			>10000	25.6	21			2154	134.6
11			>10000	26.2	22			1208	94.7
12			2754	9.8	23			4851	398.1
13			15170	63.8	24			311.6	32.1
14			1064	6.3	25			95.1	13.1
15			1810	10.8	26			56.8	9.1

^a Asterisk indicates the atom attached to the position of substitution.

function, which takes into account the effects of ligand solvation on protein–ligand association. Of the 7-azaindole derivatives tested, 12 compounds are found to have submicromolar inhibitory activity for the D816V mutant and more than 100-fold greater potency relative to wild-type c-KIT. Notably, all these highly potent and selective D816V inhibitors (**5–16**) contain a 3,4-dimethoxybenzene moiety in the 3-(Y) position of the 7-azaindole core. A comparison of the IC₅₀ values of **14** to those of **19**, **20**, **22**, and **23** clearly reveals that substitutions of other chemical groups for the 3,4-dimethoxybenzene moiety in the Y position lead to a large decrease in the inhibitory activity against the D816V mutant and a relatively insignificant change in IC₅₀ values for wild-type c-KIT. The replacement of 3,4-dimethoxybenzene at Y-position in **14** with pyridine in **25** also

leads to the decrease in selectivity. Furthermore, the introduction of 3,4-dimethoxybenzene moiety at Y-position allows specificity for inhibition of the D816V mutant to be retained for various chemical groups in the 5-(X) position of the 7-azaindole, as evidenced by the large differences between IC₅₀ values of **5–18** for wild-type c-KIT and the D816V mutant. This indicates that 3-(3,4-dimethoxyphenyl)-7-azaindole represents a good starting point for the design of the specific inhibitors of the D816V mutant.

Among the variety of substituents at the X position, a (2-aminophenyl)-morpholin-4-yl-methanone group in **5** is found to be most efficient in specifically inhibiting the D816V mutant, yielding more than 1000-fold higher potency for the mutant than for wild-type c-KIT. The highly selective inhibition of the D816V

mutant by **5**, **7**, and **8** indicates that the derivatives of 3-(3,4-dimethoxyphenyl)-7-azaindole with a large chemical group in the X position can bind tightly in the ATP-binding site of the D816V mutant and show compromised ability to be fully stabilized in the ATP-binding site of the inactive form of wild-type c-KIT. The large substituents at the X position seem to be stabilized in the internal region of the ATP-binding site because the 6-membered ring of 7-azaindole points to the center of the N-terminal domain in docking simulations (Figure 1). The relatively low potency for wild-type c-KIT of 7-azaindole inhibitors with a large substituent is actually not surprising because the volume of the ATP-binding pocket decreases in the inactive conformation due to the approach of JMR residues (residues 547-581) to the gatekeeper site.

The preference of a large chemical group at the X position for selective inhibition of the D816V mutant is further illustrated by the IC₅₀ values of **9-26** for wild-type c-KIT and the D816V mutant. For example, inhibitors with aromatic rings containing two or three substituents (**9-12**) exhibit greater selectivity than those with one or no substituent (**13-26**), except for **17**. However, the inhibitors with the same size may also exhibit a different pattern of selectivity. For example, changing the NH₂ group from *meta*- in **14** to *para*-position in **26** leads to a substantial decrease in the specificity for inhibition of the D816V mutant. Whereas the inhibitory activities of **14** and **26** with respect to the D816V mutant are similar, their IC₅₀ values with respect to wild-type c-KIT decrease significantly (**14**, IC₅₀ = 1064 nM; **26**, IC₅₀ = 56.8 nM). This indicates that the large decrease in specificity for inhibition of the D816V mutant stems from an increase in the inhibitory activity of **26** against wild-type c-KIT. Therefore, the shift of -NH₂ group from *meta*- to *para*-position is expected to cause the establishment of strong c-KIT-inhibitor interactions that enable the inhibitor to bind more tightly in the ATP-binding site of the inactive conformation of wild-type c-KIT.

The representative MD trajectory snapshots for **5** bound in the ATP-binding sites of wild-type c-KIT and the D816V mutant are compared in Figure 2. In both c-KIT-**5** and D816V-**5** complexes, the pyridinyl nitrogen of 7-azaindole ring receives a hydrogen bond from the backbone amidic nitrogen and the neighboring -NH group donates a hydrogen bond to the aminocarbonyl oxygen of Cys673. Another common structural feature of c-KIT-**5** and D816V-**5** complexes is that the carbonyl group flanking the morpholine and phenyl rings of **5** forms a hydrogen bond with the side-chain ammonium ion of Lys623. However, the third hydrogen bond in the ATP-binding site appears to be established in a different fashion in c-KIT-**5** and D816V-**5** complexes. In the c-KIT-**5** complex, the anilinic nitrogen of **5** plays the role of hydrogen bond donor with respect to the backbone aminocarbonyl oxygen of Asp810, which is a component of the highly conserved Asp-Phe-Gly (D810-F811-G812) motif in the A-loop. In the D816V-**5** complex, on the other hand, this anilinic nitrogen establishes a solvent-mediated hydrogen bond with the side-chain carboxylate group of Asp677 at the entrance of the ATP-binding site. Judging from the proximity to the 7-azaindole ring, this hydrogen bond is expected to play a role in orienting the 7-azaindole moiety in a position to form the bidentate hydrogen bonds with Cys673 in the ATP-binding site of the D816V mutant. In both c-KIT-**5** and D816V-**5** complexes, three aromatic rings of **5** appear to be stabilized

through the hydrophobic interactions with the side chains of nonpolar residues including Leu595, Val603, Ala621, Tyr672, and Leu799. In contrast, the terminal morpholine ring exhibits different binding modes in c-KIT-**5** and D816V-**5** complexes. In the D816V mutant, it is stabilized through the interactions with backbone groups of the P-loop (residues 596-602, Figure 2b). This binding mode cannot be formed in the c-KIT-**5** complex because the P-loop is too distant from the ATP-binding site. Instead, the morpholine group points toward a small hydrophobic pocket formed by the side chains of Trp557, Leu644, Val654, and Thr670 in the c-KIT-**5** complex (Figure 2a). The respective presence and absence of the interactions with the P-loop in D816V-**5** and c-KIT-**5** complexes underscore the importance of the P-loop as a key structural determinant of the binding specificity of c-KIT inhibitors. The binding mode of the terminal 3,4-dimethoxy benzene moiety also appears to be different in c-KIT-**5** and D816V-**5** complexes. It is stabilized by the interactions with Asn680 and Arg684 in the D816V-**5** complex (Figure 2b); in contrast, it is exposed to bulk solvent in the c-KIT-**5** complex (Figure 2a). This difference in binding modes can be invoked to explain the greater inhibitory activity of **5** against the D816V mutant than wild-type c-KIT.

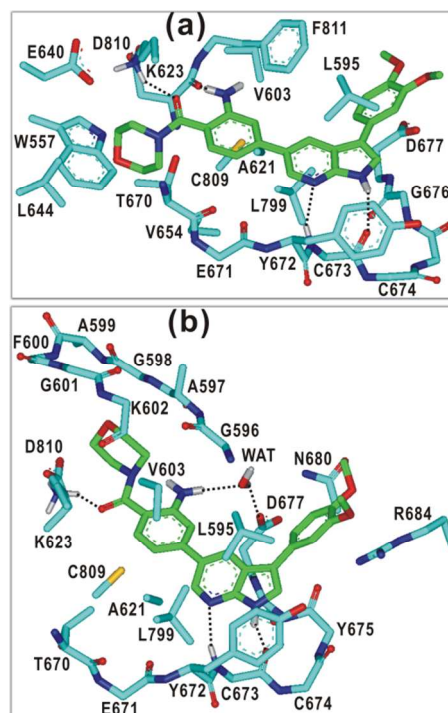


Figure 2 Representative MD trajectory snapshots of **5** in the ATP-binding sites of (a) wild-type and (b) D816V mutant of c-KIT. Carbon atoms of c-KIT and **5** are indicated in cyan and green, respectively. Dotted lines indicate a hydrogen bond.

Interestingly, compound **14** remains as a potent and specific inhibitor of the D816V mutant despite the removal of the morpholine-4-carbonyl group in **5**. The binding modes of **14** with wild-type c-KIT and the D816V mutant are similar to those of **5** in that the central 7-azaindole moiety forms the bidentate hydrogen bonds with backbone groups of Cys673, with the aromatic rings being stabilized through the hydrophobic interactions with the side chains of Leu595, Val603, Ala621,

Tyr672, and Leu799 (Figure 3). The anilinic nitrogen also forms a hydrogen bond with the backbone aminocarbonyl oxygen of Asp810 in the c-KIT-**14** complex and with that of Ala621 in the D816V-**14** complex. As in the c-KIT-**5** complex, the terminal 3,4-dimethoxy benzene group appears to be exposed to bulk solvent in the c-KIT-**14** complex. On the other hand, it is directed toward the P-loop, where it forms a water-mediated hydrogen bond with the backbone aminocarbonyl oxygen of Ala597. Thus, the number of hydrogen bonds increases from three to four in going from the wild-type receptor to the D816V mutant. Such strengthening of hydrogen bond interactions may help to explain the greater inhibitory activity of **14** for the D816V mutant than for wild-type c-KIT. Another common feature in the binding modes of **5** and **14** is that their terminal 3,4-dimethoxybenzene moiety is stabilized by protein groups at the entrance of the ATP-binding site of the D816V mutant, whereas it points to bulk solvent in the ATP-binding site of wild-type c-KIT. This difference in binding modes with respect to wild-type c-KIT and the D816V mutant confirms the effectiveness of the 3,4-dimethoxybenzene moiety in conferring high selectivity for the D816V mutant.

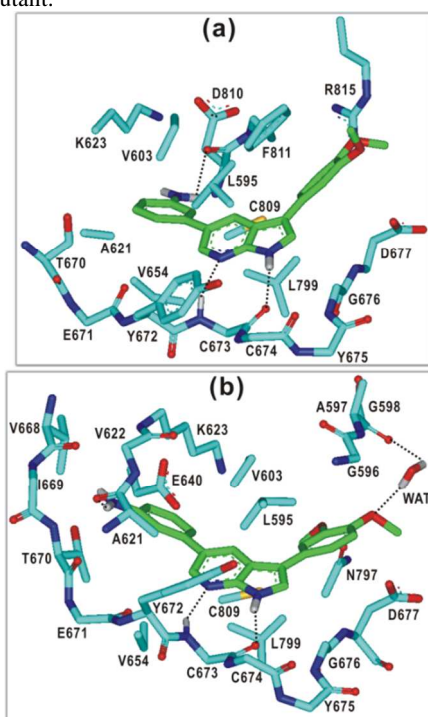


Figure 3. Representative MD trajectory snapshots of **14** in the ATP-binding sites of (a) wild-type and (b) D816V mutant of c-KIT. Carbon atoms of c-KIT and **14** are indicated in cyan and green, respectively. Each dotted line indicates a hydrogen bond.

Because the bidentate hydrogen bonds established between the 7-azaindole moiety and the backbone groups of Cys673 are the most important interactions in the wild-type c-KIT and the D816V mutant, a comparison of the dynamic stabilities of the two hydrogen bonds might shed light on the differences in inhibitory activities. A common feature of D816V-**5**, D816V-**14**, and D816V-**26** complexes is that both N \cdots H–N and N–H \cdots O hydrogen bonds between the inhibitor 7-azaindole ring and Cys673 are dynamically very stable, with an associated time-averaged distance of 1.91–1.97 Å. All six hydrogen bonds in the

three D816V-inhibitor complexes are retained for more than 99% of simulation time assuming a hydrogen bond distance limit of 2.5 Å. This dynamic stability of bidentate hydrogen bonds is actually not surprising because **5**, **14**, and **26** are found to be well-accommodated in the ATP-binding site of D816V mutant owing to the presence of P-loop residues near the entrance of the ATP-binding site. Thus, the maintenance of bidentate hydrogen bonds with dynamic stability is consistent with tight binding of inhibitors in the ATP-binding site of the D816V mutant, which helps to explain nanomolar inhibitory activities. On the other hand, the bidentate hydrogen bonds between Cys673 and the 7-azaindole ring are found to be dynamically unstable in c-KIT-**5** and c-KIT-**14** complexes as shown in Figure 4a and 4b. Although the N \cdots H–N hydrogen bond is maintained for more than 86.3% of simulation time, the residence time for the N–H \cdots O hydrogen bond fall into 72.7% in c-KIT-**5** and c-KIT-**14** complexes. These relative instabilities of the bidentate hydrogen bonds indicate that **5** and **14** would be bound weakly in the ATP-binding site of wild-type c-KIT in the inactive conformation, which is consistent with the even weaker inhibitory activities of **5** and **14** against wild-type c-KIT than against the D816V mutant. Such weak binding of **5** and **14** to wild-type c-KIT might be related to the fact that the terminal 3,4-dimethoxy benzene group is exposed to bulk solvent because the P-loop remains distant from the ATP-binding site of c-KIT in the inactive conformation, making it possible for the bidentate hydrogen bonds to be ruptured by solvent molecules. As can be seen in Figure 4c, however, the dynamic stability of the bidentate hydrogen bonds between Cys673 and the inhibitor increases significantly with a change in the substituent at the X position from 3-aminobenzene in **14** to 4-aminobenzene in **26**. The N \cdots H–N and N–H \cdots O hydrogen bonds between the inhibitor 7-azaindole ring and Cys673 exhibited residence times of 99.5% and 98.6% in the c-KIT-**26** complex. The resulting substantial increase in dynamic stability of the bidentate hydrogen bonds is consistent with the greater inhibitor potency of **26** compared with **5** and **14**, confirming a close relation between the strength of bidentate hydrogen bonds with Cys673 and inhibitory activity.

Conclusions

We have identified new 7-azaindole-based c-KIT inhibitors with nanomolar inhibitory activity and highly selective for the gain-of-function D816V mutant through the structure-based *de novo* design. Owing to improvements in the scoring function, achieved by implementing an accurate solvation free energy term, the designed derivatives are potent and selective against the D816V mutant. In particular, 7-azaindole derivatives with a 3,4-dimethoxybenzene moiety at the 3-position and a polar aromatic group at the 5-position represents a lead structure for the discovery of new anticancer agents that specifically inhibit the D816V c-KIT mutant. The results of MD simulations confirm that the strengths and dynamic stabilities of the bidentate hydrogen bonds with Cys673 serve as the critical factors affecting the potency and selectivity of c-KIT inhibitors.

Experimental

General Methods and Materials

Unless stated otherwise, reactions were performed in flame-dried

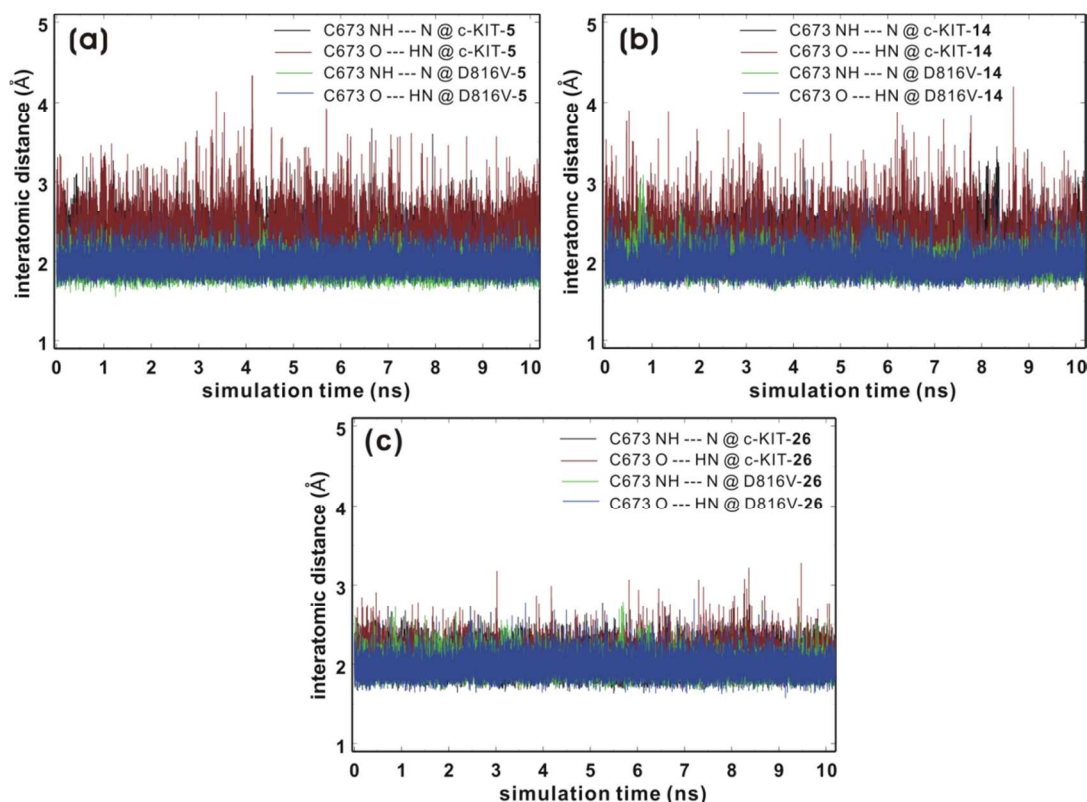


Figure 4 Time evolutions of the interatomic distances associated with the hydrogen bonds between the 7-azaindole core of (a) **5**, (b) **14**, and (c) **26** and backbone amide groups in the ATP-binding sites of wild-type c-KIT and the D816V mutant.

glassware under a positive pressure of nitrogen using freshly distilled solvents. Analytical thin layer chromatography (TLC) was performed on precoated silica gel 60 F₂₅₄ plates and visualization on TLC was achieved by UV light (254 and 354nm). Flash column chromatography was undertaken on silica gel (400-630 mesh). ¹H NMR was recorded on 600MHz, 400 MHz or 300 MHz and chemical shifts were quoted in parts per million (ppm) referenced to the appropriate solvent peak or 0.0 ppm for tetramethylsilane. The following abbreviations were used to describe peak splitting patterns when appropriate: br = broad, s = singlet, d = doublet, t = triplet, q = quartet, m = multiplet, dd = doublet of doublet. Coupling constants, *J*, were reported in hertz unit (Hz). ¹³C NMR was recorded on 100 MHz or 150MHz and was fully decoupled by broad band proton decoupling. Chemical shifts were reported in ppm referenced to the center line of a triplet at 77.0 ppm of chloroform-*d*. Mass spectral data were obtained by using EI method. Commercial grade reagents and solvents were used without further purification except as indicated below. Dichloromethane was distilled from calcium hydride. THF was distilled from sodium.

General Procedure (GP I) for Suzuki Coupling, 5-bromo-3-(3,4-dimethoxyphenyl)-1H-pyrrolo[2,3-*b*]pyridine (2). A solution of 5-bromo-3-iodo-1-(phenylsulfonyl)-1H-pyrrolo[2,3-*b*]pyridine (600 mg, 1.3 mmol), 3,4-dimethoxyphenylboronic acid (284 mg, 1.56 mmol), Cs₂CO₃ (1059 mg, 3.25 mmol) and Pd(dppf)Cl₂·CH₂Cl₂ (212 mg, 0.26 mmol) in 1,4-dioxane:H₂O = 3:1 (7 mL) was heated to 80 °C for 2 h in sealed tube.

The resulting solution was cooled to rt and 4N KOH solution (4 mL) was added. The reaction mixture was then heated to 60 °C and stirred for 1h (*N*-deprotection of benzenesulfonyl group). The mixture was diluted with water and neutralized with 6N HCl solution in ice bath. The two-phase mixture was extracted with CH₂Cl₂. The combined organic layer was dried (MgSO₄) and concentrated *in vacuo*. The residue was purified with flash column chromatography (EA / HX, gradient 1:2 to 1:1) to give the product as yellow solid (369 mg, 85%). ¹H NMR (400 MHz, Chloroform-*d*) δ 9.41 (s, 1H), 8.38 (d, *J* = 2.1 Hz, 1H), 8.28 (d, *J* = 1.8 Hz, 1H), 7.44 (d, *J* = 2.5 Hz, 1H), 7.13 (dd, *J* = 8.2, 2.0 Hz, 1H), 7.05 (d, *J* = 2.0 Hz, 1H), 6.97 (d, *J* = 8.2 Hz, 1H), 3.95 (s, 3H), 3.92 (s, 3H).

General Procedure (GP II) for Suzuki Coupling, (2-amino-4-(3-(3,4-dimethoxyphenyl)-1H-pyrrolo[2,3-*b*]pyridin-5-yl)phenyl)(morpholino)methanone (5). A solution of 5-bromo-3-(3,4-dimethoxyphenyl)-1H-pyrrolo[2,3-*b*]pyridine (90 mg, 0.267 mmol), (2-amino-4-(4,4,5,5-tetramethyl-1,3,2-dioxaborolan-2-yl)phenyl)(morpholino)methanone (107 mg, 0.321 mmol), Cs₂CO₃ (174 mg, 0.534 mmol), and PdCl₂(dppf)·CH₂Cl₂ (44 mg, 0.0534 mmol) in 1,4-dioxane/H₂O = 3:1 (2 mL) was charged in capped tube and was heated to 100 °C for 3h. The reaction mixture was cooled to room temperature and concentrated *in vacuo*. The residue was diluted with CH₂Cl₂ and organic phase was extracted with CH₂Cl₂. The combined organic layer was dried with MgSO₄ and concentrated *in vacuo*. The mixture was purified with flash column chromatography (CH₂Cl₂ / MeOH, gradient 20:1 to 15:1) to give the product as pale yellow solid

(52.4 mg, 43%). mp 153 - 157 °C. ¹H NMR (400 MHz, DMSO-*d*₆) δ 11.90 (s, 1H), 8.51 (d, *J* = 2.2 Hz, 1H), 8.33 (d, *J* = 2.2 Hz, 1H), 7.82 (t, *J* = 2.1 Hz, 1H), 7.28-7.25 (m, 2H), 7.12 (d, *J* = 7.9 Hz, 1H), 7.09 (s, 1H), 7.03 (d, *J* = 8.1 Hz, 1H), 6.96 (dd, *J* = 7.9, 1.7 Hz, 1H), 5.34 (s, 2H), 3.84 (s, 3H), 3.77 (s, 3H) 3.61(s, 4H). ¹³C NMR (100MHz, DMSO-*d*₆) δ 168.62, 149.19, 148.64, 147.33, 146.45, 141.62, 140.81, 128.75, 128.42, 127.75, 125.00, 123.98, 118.66, 117.61, 117.41, 114.85, 114.43, 113.77, 112.45, 110.69, 66.19, 55.63, 55.60. HRMS (EI+) *m/z* calcd for C₂₆H₂₆N₄O₄ [M + Na]⁺, 481.1852; found 481.1866.

3-(3-(3,4-dimethoxyphenyl)-1H-pyrrolo[2,3-*b*]pyridin-5-yl)-*N,N*-dimethylaniline (6). Compound **6** was prepared (13.7 mg, 30%) according to GP II (EA / HX, gradient 1:1) from 5-bromo-3-(3,4-dimethoxyphenyl)-1H-pyrrolo[2,3-*b*]pyridine (40 mg, 0.122 mmol) and (3-(dimethylamino)phenyl) boronic acid (24.2 mg, 0.146 mmol) as white solid. mp 213 – 215 °C. ¹H NMR (400 MHz, DMSO-*d*₆) δ 11.85 (s, 1H), 8.51 (d, *J* = 2.1 Hz, 1H), 8.33 (d, *J* = 2.1 Hz, 1H), 7.80 (d, *J* = 2.5 Hz, 1H), 7.29 – 7.21 (m, 3H), 7.03 (d, *J* = 8.8 Hz, 1H), 6.99 – 6.94 (m, 2H), 6.72 (d, *J* = 7.5 Hz, 1H), 3.84 (s, 3H), 3.77 (s, 3H) 2.95 (s, 6H). ¹³C NMR (100 MHz, DMSO-*d*₆) δ 150.93, 149.13, 148.50, 147.20, 141.96, 139.85, 129.63, 129.44, 127.85, 125.33, 123.76, 118.53, 117.28, 115.17, 114.70, 112.50, 111.12, 111.09, 110.55, 55.58, 55.49, 40.21. HRMS (EI+) *m/z* calcd for C₂₃H₂₃N₃O₂ [M + H]⁺, 374.1869; found 374.1845.

General Procedure (GP III) for Suzuki Coupling. (3-amino-5-(3-(3,4-dimethoxyphenyl)-1H-pyrrolo[2,3-*b*]pyridin-5-yl)phenyl)(morpholino)methanone (7). A solution of 5-bromo-3-(3,4-dimethoxyphenyl)-1H-pyrrolo[2,3-*b*]pyridine (75 mg, 0.23 mmol), bis(pinacolato)diboron (74.6mg, 0.29 mmol), KOAc (44.4 mg, 0.452 mmol) and Pd(dppf)Cl₂·CH₂Cl₂ (37 mg, 0.045 mmol) in anhydrous 1,4-dioxane was heated to 90 °C for 12 h under an atmosphere of N₂. The reaction mixture was cooled to RT and concentrated *in vacuo*. The residue was diluted with CH₂Cl₂ and MeOH and then filtered through a short pad of silica (SiO₂) and celite eluting with CH₂Cl₂ and MeOH (15:1). The filtrate was concentrated *in vacuo* then purified by flash column chromatography(EA / HX, gradient 1:3 to 1:1) to give **3** as brown solid (63.9 mg, 74%). ¹H NMR (300 MHz, Chloroform-*d*) δ 12.14 (s, 1H), 8.82 (d, *J* = 1.4 Hz, 1H), 8.68 (d, *J* = 1.4 Hz, 1H), 7.54 (s, 1H), 7.28 (dd, *J* = 8.3, 2.0 Hz, 1H), 7.17 (t, *J* = 2.5 Hz, 1H), 7.02 (d, *J* = 8.3 Hz, 1H), 3.99 (s, 3H), 3.96 (s, 3H), 1.41(s, 12H). A solution of **3** (23 mg, 0.06 mmol), (3-amino-5-bromophenyl)(morpholino)methanone (20.5 mg, 0.072 mmol), Cs₂CO₃ (39.1 mg, 0.12 mmol) and Pd(dppf)Cl₂·CH₂Cl₂ (12.2 mg, 0.015 mmol) in 1,4-dioxane/H₂O = 3:1 (1.5 mL) was charged in capped tube and was heated to 100 °C for 3 h. The reaction mixture was cooled to room temperature and concentrated *in vacuo*. The residue was diluted with CH₂Cl₂ and organic phase was extracted with CH₂Cl₂. The combined organic layer was dried with MgSO₄ and concentrated *in vacuo*. The mixture was purified with flash column chromatography (CH₂Cl₂ / MeOH, gradient 30:1 to 15:1) to give the product as pale yellow solid (6 mg, 22%). mp 154 - 157 °C. ¹H NMR (400 MHz, DMSO-*d*₆) δ 11.88 (s, 1H), 8.46 (d, *J* = 2.0 Hz, 1H), 8.27 (d, *J* = 2.1Hz, 1H), 7.82 (d, *J* = 2.3Hz, 1H), 7.28 – 7.24 (m, 2H), 7.04 (d, *J* = 8.2 Hz, 1H), 6.95 (d, *J* = 2.1 Hz, 1H), 6.82 (d, *J* = 1.9 Hz, 1H), 6.55 (s, 1H), 5.39 (s, 2H), 3.84 (s, 3H), 3.78 (s, 3H), 3.59 (br, 8H). ¹³C

NMR (150 MHz, DMSO-*d*₆) δ 169.59, 149.34, 149.19, 148.55, 147.33, 141.65, 139.83, 137.08, 128.64, 127.76, 125.05, 123.93, 118.66, 117.36, 114.81, 113.18, 112.67, 112.51, 110.85, 110.72, 66.17, 55.63, 40.04. HRMS (EI+) *m/z* calcd for C₂₆H₂₆N₄O₄ [M + Na]⁺, 481.1852; found 481.1860.

5-(3-(3,4-dimethoxyphenyl)-1H-pyrrolo[2,3-*b*]pyridin-5-yl)-2-(2-morpholinoethoxy)aniline (8). Compound **8** was prepared (12.9 mg, 30%) according to GP III (CH₂Cl₂ / MeOH, gradient 30:1 to 15:1) from **3** (35 mg, 0.092 mmol) and 5-bromo-2-(2-morpholinoethoxy)aniline as white solid. mp 96 – 98 °C. ¹H NMR (400 MHz, Chloroform-*d*) δ 9.48 (s, 1H), 8.52 (s, 1H), 8.26 (d, *J* = 1.9 Hz, 1H), 7.44 (d, *J* = 2.2 Hz, 1H), 7.20 (dd, *J* = 8.2, 2.0 Hz, 1H), 7.12 (d, *J* = 2.0 Hz, 1H), 6.98 – 6.88 (m, 4H), 4.17 (t, *J* = 5.6 Hz, 2H), 3.94 (s, 3H), 3.92(s, 3H), 3.73 (t, *J* = 4.6Hz, 4H), 2.82 (t, *J* = 5.6 Hz, 2H), 2.59 (t, *J* = 4.3Hz, 4H). ¹³C NMR (150 MHz, Chloroform-*d*) δ 149.39, 148.17, 148.00, 145.87, 142.76, 137.38, 133.35, 130.35, 127.74, 126.21, 121.79, 119.68, 118.43, 117.38, 116.91, 114.24, 113.31, 111.87, 110.92, 66.98, 66.83, 57.84, 56.08, 56.06, 54.04. HRMS (EI+) *m/z* calcd for C₂₇H₃₀N₄O₄ [M + H]⁺, 475.2345; found 475.2350.

5-(3-(3,4-dimethoxyphenyl)-1H-pyrrolo[2,3-*b*]pyridin-5-yl)-2-methylaniline (9). Compound **9** was prepared (31.8 mg, 57%) according to GP II (CH₂Cl₂ / MeOH, gradient 60:1 to 30:1) from 5-bromo-3-(3,4-dimethoxyphenyl)-1H-pyrrolo[2,3-*b*]pyridine (50 mg, 0.15 mmol) and 2-methyl-5-(4,4,5,5-tetramethyl-1,3,2-dioxaborolan-2-yl)aniline (42 mg, 0.18 mmol) as white solid. mp 170 – 174 °C. ¹H NMR(400 MHz, DMSO-*d*₆) δ 11.82 (d, *J* = 2.6 Hz, 1H), 8.44 (d, *J* = 2.1 Hz, 1H), 8.24 (d, *J* = 2.1 Hz, 1H), 7.79 (d, *J* = 2.6 Hz, 1H), 7.26 – 7.23 (m, 2H), 7.02 (dd, *J* = 10.24, 7.65 Hz, 2H), 6.95 (d, *J* = 1.9 Hz, 1H), 6.82 (dd, *J* = 7.6, 1.9 Hz, 1H), 4.91 (s, 2H), 3.84 (s, 3H), 3.78 (s, 3H), 2.08 (s, 3H). ¹³C NMR (100 MHz, DMSO-*d*₆) δ 149.15, 148.31, 147.23, 147.04, 141.55, 137.22, 130.52, 129.32, 127.87, 124.56, 123.73, 120.04, 118.54, 117.36, 114.74, 114.62, 112.46, 112.36, 110.60, 55.61, 55.58, 17.08. HRMS (EI+) *m/z* calcd for C₂₂H₂₁N₃O₂ [M + H]⁺, 360.1712; found 360.1691.

5-(3-(3,4-dimethoxyphenyl)-1H-pyrrolo[2,3-*b*]pyridin-5-yl)-2-methoxyaniline (10). Compound **10** was prepared (44.2 mg, 39%) according to GP II (CH₂Cl₂ / MeOH, gradient 30:1) from 5-bromo-3-(3,4-dimethoxyphenyl)-1H-pyrrolo[2,3-*b*]pyridine (100 mg, 0.3 mmol) and 2-methoxy-5-(4,4,5,5-tetramethyl-1,3,2-dioxaborolan-2-yl)aniline (89.7 mg, 0.36 mmol) as white solid. mp 193 – 195 °C. ¹H NMR (400 MHz, Chloroform-*d*) δ 10.98 (s, 1H), 8.52 (d, *J* = 2.0 Hz, 1H), 8.27 (d, *J* = 2.0 Hz, 1H), 7.46 (s, 1H), 7.19 (dd, *J* = 8.2, 2.0 Hz, 1H), 7.13 (d, *J* = 2.0 Hz, 1H), 6.97 – 6.95 (m, 3H), 6.87 (dd, *J* = 8.1, 1.2 Hz, 1H), 3.92 (s,3H), 3.92 (s, 3H), 3.89 (s, 3H). ¹³C NMR (100 MHz, Chloroform-*d*) δ 149.32, 148.28, 147.80, 146.84, 142.04, 136.55, 132.61, 130.11, 127.94, 126.26, 122.31, 119.55, 118.59, 117.38, 116.37, 114.00, 111.82, 110.81, 110.77, 56.02, 55.99, 55.63. HRMS (EI+) *m/z* calcd for C₂₂H₂₁N₃O₃ [M + H]⁺, 376.1661; found 376.1635

3-(3-(3,4-dimethoxyphenyl)-1H-pyrrolo[2,3-*b*]pyridin-5-yl)-5-methoxyaniline (11). Compound **11** was prepared (40.8 mg, 36%) according to GP II (EA / HX 3:1) from 5-bromo-3-(3,4-dimethoxyphenyl)-1H-pyrrolo[2,3-*b*]pyridine (100 mg, 0.3 mmol) and 3-methoxy-5-(4,4,5,5-tetramethyl-1,3,2-dioxaborolan-2-yl)aniline (89.7 mg, 0.36 mmol) as white solid. mp 190 – 195 °C. ¹H NMR(400 MHz, DMSO-*d*₆) δ 11.86 (d, *J* = 1.8 Hz, 1H), 8.47

(d, $J = 2.1$ Hz, 1H), 8.27 (d, $J = 2.1$ Hz, 1H), 7.81 (d, $J = 2.5$ Hz, 1H), 7.28 – 7.26 (m, 2H), 7.04 (d, $J = 8.8$ Hz, 1H), 6.51 (t, $J = 1.7$ Hz, 1H), 6.44 (dd, $J = 2.4, 1.5$ Hz, 1H), 6.16 (t, $J = 2.0$ Hz, 1H), 5.19 (s, 2H), 3.85 (s, 3H), 3.78 (s, 3H), 3.73 (s, 3H). ^{13}C NMR (100 MHz, DMSO- d_6) δ 160.78, 150.33, 149.17, 148.52, 147.26, 141.69, 140.62, 129.36, 127.84, 124.90, 123.78, 118.57, 117.28, 114.70, 112.49, 110.65, 105.63, 100.66, 98.17, 55.60, 55.57, 54.74. HRMS (EI+) m/z calcd for $\text{C}_{22}\text{H}_{21}\text{N}_3\text{O}_3$ [M + H] $^+$, 376.1661; found 376.1643

10 3-(3,4-dimethoxyphenyl)-5-(3,4,5-trimethoxyphenyl)-1H-pyrrolo[2,3-b]pyridine (12). Compound **12** was prepared (37 mg, 59%) according to GP II (EA / HX, 2:1) from 5-bromo-3-(3,4-dimethoxyphenyl)-1H-pyrrolo[2,3-b]pyridine (50 mg, 0.15 mmol) and (3,4,5-trimethoxyphenyl) boronic acid (38.2 mg, 0.18 mmol) as white solid. mp 202 – 204 °C. ^1H NMR (400 MHz, DMSO- d_6) δ 11.89 (s, 1H), 8.57 (d, $J = 2.1$ Hz, 1H), 8.40 (d, $J = 2.1$ Hz, 1H), 7.82 (d, $J = 2.2$ Hz, 1H), 7.32 – 7.29 (m, 2H), 7.02 (d, $J = 8.1$ Hz, 1H), 6.99 (s, 2H), 3.87 (s, 6H), 3.86 (s, 3H), 3.78 (s, 3H), 3.70 (s, 3H). ^{13}C NMR (100 MHz, DMSO- d_6) δ 153.27, 149.15, 148.51, 147.22, 142.03, 136.80, 134.98, 128.91, 127.85, 125.49, 123.87, 118.59, 117.24, 114.78, 112.52, 110.59, 104.66, 60.04, 56.00, 55.61, 55.49. HRMS (EI+) m/z calcd for $\text{C}_{24}\text{H}_{24}\text{N}_2\text{O}_5$ [M + Na] $^+$, 443.1583; found 443.1566.

11 3-(3-(3,4-dimethoxyphenyl)-1H-pyrrolo[2,3-b]pyridin-5-yl)benzotrile (13). Compound **13** was prepared (31.5 mg, 59%) according to GP II (EA / HX, gradient 1:1) from 5-bromo-3-(3,4-dimethoxyphenyl)-1H-pyrrolo[2,3-b]pyridine (50 mg, 0.15 mmol) and (3-cyanophenyl)boronic acid (26.4 mg, 0.18 mmol) as white solid. mp 198 – 206 °C. ^1H NMR (400 MHz, DMSO- d_6) δ 11.98 (d, $J = 2.7$ Hz, 1H), 8.61 (d, $J = 2.1$ Hz, 1H), 8.49 (d, $J = 2.2$ Hz, 1H), 8.30 (s, 1H), 8.12 (ddd, $J = 7.9, 2.0, 1.1$ Hz, 1H), 7.86 (d, $J = 2.6$ Hz, 1H), 7.81 (dt, $J = 7.8, 1.3$ Hz, 1H), 7.67 (t, $J = 7.8$ Hz, 1H), 7.35 (dd, $J = 8.2, 2.0$ Hz, 1H), 7.27 (d, $J = 2.0$ Hz, 1H), 7.03 (d, $J = 8.3$ Hz, 1H), 3.85 (s, 3H), 3.78 (s, 3H). ^{13}C NMR (100 MHz, DMSO- d_6) δ 149.15, 148.84, 147.34, 141.87, 140.31, 131.82, 130.56, 130.44, 130.07, 127.57, 126.50, 125.89, 124.24, 118.89, 118.81, 117.39, 115.10, 112.43, 112.08, 110.70, 55.59. HRMS (EI+) m/z calcd for $\text{C}_{22}\text{H}_{17}\text{N}_3\text{O}_2$ [M + Na] $^+$, 378.1218; found 378.1217

12 3-(3-(3,4-dimethoxyphenyl)-1H-pyrrolo[2,3-b]pyridin-5-yl)aniline (14). Compound **14** was prepared (11 mg, 25%) according to GP II (CH_2Cl_2 / MeOH, gradient 30:1) from 5-bromo-3-(3,4-dimethoxyphenyl)-1H-pyrrolo[2,3-b]pyridine (40 mg, 0.12 mmol) and 3-aminophenylboronic acid (20 mg, 0.15 mmol) as white solid. mp 200 – 203 °C. ^1H NMR (400 MHz, Chloroform- d) δ 10.57 (s, 1H), 8.56 (d, $J = 2.0$ Hz, 1H), 8.32 (d, $J = 2.0$ Hz, 1H), 7.48 (s, 1H), 7.25 (t, $J = 7.8$ Hz, 1H), 7.20 (dd, $J = 8.3, 2.0$ Hz, 1H), 7.13 (d, $J = 2.0$ Hz, 1H), 7.01 (dt, $J = 7.8, 1.1$ Hz, 1H), 6.97 (d, $J = 8.2$ Hz, 1H), 6.92 (t, $J = 2.1$ Hz, 1H), 6.69 (dt, $J = 7.9, 1.6$ Hz, 1H), 3.93 (s, 3H), 3.92 (s, 3H), 3.00 (br, 2H). ^{13}C NMR (150 MHz, Chloroform- d) δ 149.39, 148.61, 147.94, 146.93, 142.46, 140.76, 130.28, 129.90, 127.80, 126.61, 122.22, 119.64, 118.56, 117.86, 116.73, 114.07, 113.89, 111.87, 110.85, 56.05. HRMS (EI+) m/z calcd for $\text{C}_{21}\text{H}_{19}\text{N}_3\text{O}_2$ [M + H] $^+$, 346.1556; found 346.1543

13 5-(3-(3,4-dimethoxyphenyl)-1H-pyrrolo[2,3-b]pyridin-5-yl)pyridin-3-amine (15). Compound **15** was prepared (42.6 mg, 40%) according to GP II (CH_2Cl_2 / MeOH, gradient 20:1 to 15:1)

from 5-bromo-3-(3,4-dimethoxyphenyl)-1H-pyrrolo[2,3-b]pyridine (101 mg, 0.3 mmol) and 5-(4,4,5,5-tetramethyl-1,3,2-dioxaborolan-2-yl)pyridin-3-amine (81 mg, 0.368 mmol) as white solid. mp 254 – 260 °C. ^1H NMR (400 MHz, DMSO- d_6) δ 11.96 (s, 1H), 8.49 (s, 1H), 8.33 (s, 1H), 8.12 (s, 1H), 7.94 (s, 1H), 7.86 (s, 1H), 7.29 (d, $J = 8.2$ Hz, 1H), 7.24 (d, $J = 13.4$ Hz, 2H), 7.02 (d, $J = 8.2$ Hz, 1H), 5.42 (s, 2H), 3.84 (s, 3H), 3.78 (s, 3H). ^{13}C NMR (100 MHz, DMSO- d_6) δ 149.16, 148.67, 147.30, 144.92, 141.52, 135.42, 135.06, 134.61, 127.67, 126.28, 125.25, 124.05, 118.66, 117.89, 117.44, 114.81, 112.44, 110.65, 55.59. HRMS (EI+) m/z calcd for $\text{C}_{20}\text{H}_{18}\text{N}_4\text{O}_2$ [M + H] $^+$, 347.1508; found 347.1508

14 3-(3,4-dimethoxyphenyl)-5-(*m*-tolyl)-1H-pyrrolo[2,3-b]pyridine (16). Compound **16** was prepared (9.9 mg, 60%) according to GP II (CH_2Cl_2 / MeOH, gradient 60:1 to 30:1) from 5-bromo-3-(3,4-dimethoxyphenyl)-1H-pyrrolo[2,3-b]pyridine (16 mg, 0.048 mmol) and *m*-tolylboronic acid (7.8 mg, 0.58 mmol) as white solid. mp 184 – 190 °C. ^1H NMR (400 MHz, DMSO- d_6) δ 11.87 (s, 1H), 8.52 (d, $J = 2.1$ Hz, 1H), 8.34 (d, $J = 2.1$ Hz, 1H), 7.81 (s, 1H), 7.54 (s, 1H), 7.51 (dd, $J = 8.2, 1.6$ Hz, 1H), 7.36 (t, $J = 7.6$ Hz, 1H), 7.29 (dd, $J = 8.2, 2.1$ Hz, 1H), 7.25 (d, $J = 2.0$ Hz, 1H), 7.17 (ddt, $J = 7.6, 1.8, 0.9$ Hz, 1H), 7.03 (d, $J = 8.3$ Hz, 1H), 3.84 (s, 3H), 3.77 (s, 3H), 2.38 (s, 3H). ^{13}C NMR (100 MHz, DMSO- d_6) δ 149.15, 148.49, 147.26, 141.82, 139.01, 138.11, 128.84, 128.68, 127.77, 127.69, 127.52, 125.21, 124.13, 123.89, 118.65, 117.37, 114.79, 112.47, 110.65, 55.59, 55.56, 21.10. HRMS (EI+) m/z calcd for $\text{C}_{22}\text{H}_{20}\text{N}_2\text{O}_2$ [M + Na] $^+$, 367.1422; found 367.1423

15 3,5-bis(3,4-dimethoxyphenyl)-1H-pyrrolo[2,3-b]pyridine (17). Compound **17** was prepared (27 mg, 58%) according to GP II (EA / HX 2:1) from 5-bromo-3-(3,4-dimethoxyphenyl)-1H-pyrrolo[2,3-b]pyridine (40 mg, 0.12 mmol) and 3,4-dimethoxyphenylboronic acid (26.2 mg, 0.14 mmol) as white solid. mp 218 – 223 °C. ^1H NMR (400 MHz, DMSO- d_6) δ 11.86 (d, $J = 2.6$ Hz, 1H), 8.54 (d, $J = 2.1$ Hz, 1H), 8.35 (d, $J = 2.1$ Hz, 1H), 7.81 (d, $J = 2.5$ Hz, 1H), 7.31 – 7.28 (m, 3H), 7.24 (dd, $J = 8.3, 2.1$ Hz, 1H), 7.03 (dd, $J = 8.6, 7.1$ Hz, 2H), 3.86 (s, 3H), 3.86 (s, 3H), 3.79 (s, 3H), 3.78 (s, 3H). ^{13}C NMR (100 MHz, DMSO- d_6) δ 149.18, 149.15, 148.32, 148.16, 147.21, 141.81, 131.94, 128.71, 127.89, 125.01, 123.80, 119.13, 118.58, 117.33, 114.70, 112.48, 112.38, 110.98, 110.57, 55.60, 55.52. HRMS (EI+) m/z calcd for $\text{C}_{23}\text{H}_{22}\text{N}_2\text{O}_4$ [M + Na] $^+$, 413.1477; found 413.1482

16 3-(3,4-dimethoxyphenyl)-5-(pyridin-3-yl)-1H-pyrrolo[2,3-b]pyridine (18). Compound **18** was prepared (31 mg, 62%) according to GP II (CH_2Cl_2 / MeOH, gradient 30:1 to 15:1) from 5-bromo-3-(3,4-dimethoxyphenyl)-1H-pyrrolo[2,3-b]pyridine (50 mg, 0.15 mmol) and 3-pyridinylboronic acid (22.1 mg, 0.18 mmol) as white solid. mp 225 – 226 °C. ^1H NMR (400 MHz, DMSO- d_6) δ 12.00 (s, 1H), 8.99 (d, $J = 2.4$ Hz, 1H), 8.60 (d, $J = 2.2$ Hz, 1H), 8.57 (dd, $J = 4.9, 1.6$ Hz, 1H), 8.47 (d, $J = 2.1$ Hz, 1H), 8.17 (dt, $J = 7.9, 2.0$ Hz, 1H), 7.87 (d, $J = 2.4$ Hz, 1H), 7.48 (dd, $J = 7.9, 4.8$ Hz, 1H), 7.33 (dd, $J = 8.1, 2.1$ Hz, 1H), 7.29 (d, $J = 2.1$ Hz, 1H), 7.02 (d, $J = 8.2$ Hz, 1H), 3.85 (s, 3H), 3.78 (s, 3H). ^{13}C NMR (100 MHz, DMSO- d_6) δ 149.18, 148.80, 147.94, 147.34, 141.78, 134.66, 134.45, 127.63, 125.79, 125.46, 124.19, 123.85, 118.77, 117.49, 115.00, 112.44, 110.67, 55.60, 55.58. HRMS (EI+) m/z calcd for $\text{C}_{20}\text{H}_{17}\text{N}_3\text{O}_2$ [M + H] $^+$, 332.1399; found 332.1385

3-(5-(3-aminophenyl)-1H-pyrrolo[2,3-b]pyridin-3-yl)benzotrile (19). 3-(5-Bromo-1H-pyrrolo[2,3-b]pyridin-3-yl)benzotrile was prepared (54 mg, 84%) according to GP I from 5-bromo-3-iodo-1-(phenyl-sulfonyl)-1H-pyrrolo[2,3-b]pyridine (100 mg, 0.216 mmol) and 3-cyanophenylboronic acid (33 mg, 0.22 mmol). ¹H NMR (300 MHz, DMSO-*d*₆) δ 12.38 (s, 1H), 8.59 (d, *J* = 2.1 Hz, 1H), 8.35 (d, *J* = 2.1 Hz, 1H), 8.07–8.19 (m, 3H), 7.59–7.70 (m, 2H). Compound **19** was prepared (16 mg, 39 %) according to GP II (CH₂Cl₂ / MeOH, gradient 30:1 to 15:1) from 3-(5-bromo-1H-pyrrolo[2,3-b]pyridin-3-yl)benzotrile (40 mg, 0.13 mmol) and 3-aminophenylboronic acid (21 mg, 0.15 mmol) as pale yellow solid. mp 221 – 223 °C. ¹H NMR (400 MHz, DMSO-*d*₆) δ 12.13 (s, 1H), 8.48 (d, *J* = 2.0 Hz, 1H), 8.38 (d, *J* = 2.1 Hz, 1H), 8.21 (d, *J* = 1.8 Hz, 1H), 8.14 (dd, *J* = 7.7, 1.7 Hz, 1H), 8.09 (s, 1H), 7.70–7.62 (m, 2H), 7.13 (t, *J* = 7.8 Hz, 1H), 6.91 (s, 1H), 6.88 (d, *J* = 8.0 Hz, 1H), 6.58 (dd, *J* = 7.9, 2.3 Hz, 1H), 5.15 (s, 2H). ¹³C NMR (100 MHz, DMSO-*d*₆) δ 149.13, 148.49, 142.16, 139.49, 136.37, 130.78, 130.09, 129.44, 129.35, 129.04, 125.89, 125.05, 119.04, 116.84, 114.89, 112.79, 112.61, 112.51, 112.06. HRMS (EI+) *m/z* calcd for C₂₀H₁₄N₄ [M + Na]⁺, 333.1116; found, 333.1101

3-(3-(3-fluoro-4-methoxyphenyl)-1H-pyrrolo[2,3-b]pyridin-5-yl)aniline (20). 5-bromo-3-(3-fluoro-4-methoxyphenyl)-1H-pyrrolo[2,3-b]pyridine was prepared (85.1 mg, 61 %) according to GP I from 5-bromo-3-iodo-1-(phenyl-sulfonyl)-1H-pyrrolo[2,3-b]pyridine (200 mg, 0.432 mmol) and 3-fluoro-4-methoxyphenylboronic acid (88.1 mg, 0.518 mmol). ¹H NMR (400 MHz, Chloroform-*d*) δ 9.79 (s, 1H), 8.38 (dd, *J* = 2.1, 0.4 Hz, 1H), 8.28 (dd, *J* = 2.1, 0.7 Hz, 1H), 7.44 (d, *J* = 2.5 Hz, 1H), 7.32–7.28 (m, 1H), 7.28–7.26 (m, 1H), 7.04 (t, *J* = 8.8 Hz, 1H), 3.93 (s, 3H). Compound **20** was prepared (37 mg, 46.1 %) according to GP II (EA / HX, gradient 2:1) from 5-bromo-3-(3-fluoro-4-methoxyphenyl)-1H-pyrrolo[2,3-b]pyridine (77.3 mg, 0.24 mmol) and 3-aminophenylboronic acid (44.8 mg, 0.29 mmol) as white solid. mp 199 – 201 °C. ¹H NMR (400 MHz, DMSO-*d*₆) δ 11.93 (s, 1H), 8.47 (d, *J* = 2.1 Hz, 1H), 8.28 (d, *J* = 2.1 Hz, 1H), 7.86 (d, *J* = 2.0 Hz, 1H), 7.58 (dd, *J* = 12.9, 2.1 Hz, 1H), 7.53 (ddd, *J* = 8.5, 2.2, 1.0 Hz, 1H), 7.23 (t, *J* = 8.9 Hz, 1H), 7.12 (t, *J* = 7.8 Hz, 1H), 6.91 (t, *J* = 2.0 Hz, 1H), 6.87 (ddd, *J* = 7.6, 1.8, 0.9 Hz, 1H), 6.57 (ddd, *J* = 7.9, 2.2, 0.9 Hz, 1H), 5.15 (s, 2H), 3.86 (s, 3H). ¹³C NMR (100 MHz, DMSO-*d*₆) δ 151.87 (d, *J* = 243.2 Hz), 149.15, 148.42, 145.21 (d, *J* = 10.7 Hz), 141.83, 139.58, 129.62, 129.47, 128.26 (d, *J* = 7.0 Hz), 124.81, 124.33, 122.39 (d, *J* = 3.3 Hz), 117.08, 114.75, 114.43 (d, *J* = 2.3 Hz), 113.84 (d, *J* = 18.4 Hz), 113.33 (d, *J* = 1.9 Hz), 112.75, 112.50, 56.05. HRMS (EI+) *m/z* calcd for C₂₀H₁₆FN₃O [M + H]⁺, 334.1356; found, 334.1326

3-(3,4-dimethoxyphenyl)-5-phenyl-1H-pyrrolo[2,3-b]pyridine (21). Compound **21** was prepared (42.4 mg, 43%) according to GP II (EA / CH₂Cl₂, gradient 1:5 to 1:3) from 5-bromo-3-(3,4-dimethoxyphenyl)-1H-pyrrolo[2,3-b]pyridine (99 mg, 0.3 mmol) and phenylboronic acid (43.9 mg, 0.36 mmol) as white solid. mp 192 – 194 °C. ¹H NMR (400 MHz, Chloroform-*d*) δ 11.19 (s, 1H), 8.62 (d, *J* = 2.1 Hz, 1H), 8.37 (d, *J* = 2.0 Hz, 1H), 7.67–7.61 (m, 2H), 7.53 (d, *J* = 1.9 Hz, 1H), 7.48 (t, *J* = 7.6 Hz, 2H), 7.37 (t, *J* = 7.4 Hz, 1H), 7.22 (dd, *J* = 8.2, 2.0 Hz, 1H), 7.15 (d, *J* = 2.0 Hz, 1H), 6.98 (d, *J* = 8.2 Hz, 1H), 3.94 (s, 3H), 3.93 (s, 3H). ¹³C NMR (100 MHz, DMSO-*d*₆) δ 149.17, 148.55, 147.29, 141.83,

139.09, 128.98, 128.60, 127.77, 127.05, 126.89, 125.32, 123.96, 118.68, 117.42, 114.85, 112.47, 110.64, 55.59. HRMS (EI+) *m/z* calcd for C₂₁H₁₈N₂O₂ [M + Na]⁺, 353.1266; found 353.1253.

3-(3-(3,4,5-trimethoxyphenyl)-1H-pyrrolo[2,3-b]pyridin-5-yl)aniline (22). 5-bromo-3-(3,4,5-trimethoxyphenyl)-1H-pyrrolo[2,3-b]pyridine was prepared (91 mg, 77%) according to GP I from 5-bromo-3-iodo-1-(phenyl-sulfonyl)-1H-pyrrolo[2,3-b]pyridine (150 mg, 0.325 mmol) and (3,4,5-trimethoxyphenyl)boronic acid (82.6 mg, 0.390 mmol). ¹H NMR (400 MHz, Chloroform-*d*) δ 9.62 (s, 1H), 8.39 (s, 1H), 8.27 (d, *J* = 1.9 Hz, 1H), 7.46 (d, *J* = 2.3 Hz, 1H), 6.75 (s, 2H), 3.93 (s, 6H), 3.89 (s, 3H). Compound **22** was prepared (42.3 mg, 47 %) according to GP II (EA / HX 2:1) 5-bromo-3-(3,4,5-trimethoxyphenyl)-1H-pyrrolo[2,3-b]pyridine (87 mg, 0.24 mmol) and 3-aminophenylboronic acid (44.5 mg, 0.29 mmol) as white solid. mp 206 – 208 °C. ¹H NMR (400 MHz, DMSO-*d*₆) δ 11.92 (d, *J* = 2.7 Hz, 1H), 8.47 (d, *J* = 2.0 Hz, 1H), 8.29 (d, *J* = 2.1 Hz, 1H), 7.86 (d, *J* = 2.6 Hz, 1H), 7.12 (t, *J* = 7.8 Hz, 1H), 6.95 (s, 2H), 6.91 (t, *J* = 2.0 Hz, 1H), 6.87 (ddd, *J* = 7.5, 1.9, 1.0 Hz, 1H), 6.56 (ddd, *J* = 8.0, 2.2, 0.9 Hz, 1H), 5.18 (s, 2H), 3.87 (s, 6H), 3.69 (s, 3H). ¹³C NMR (100 MHz, DMSO-*d*₆) δ 153.26, 149.16, 148.41, 141.74, 139.56, 135.94, 130.66, 129.51, 129.41, 124.74, 124.42, 117.28, 114.92, 114.53, 112.69, 112.35, 104.07, 60.05, 55.97. HRMS (EI+) *m/z* calcd for C₂₂H₂₁N₃O₃ [M + Na]⁺, 398.1481; found 398.1471.

3-(3-(4-methoxyphenyl)-1H-pyrrolo[2,3-b]pyridin-5-yl)aniline (23). 5-bromo-3-(4-methoxyphenyl)-1H-pyrrolo[2,3-b]pyridine was prepared (118 mg, 60%) according to GP I from 5-bromo-3-iodo-1-(phenyl-sulfonyl)-1H-pyrrolo[2,3-b]pyridine (300 mg, 0.649 mmol) and 4-methoxyphenylboronic acid (118.4 mg, 0.78 mmol). ¹H NMR (300 MHz, Chloroform-*d*) δ 9.29 (s, 3H), 8.36 (dd, *J* = 2.1, 0.4 Hz, 1H), 8.28 (dd, *J* = 2.1, 0.7 Hz, 1H), 7.49 (d, *J* = 8.9 Hz, 2H), 7.41 (d, *J* = 2.6 Hz, 1H), 7.00 (d, *J* = 8.8 Hz, 2H), 3.85 (s, 3H). Compound **23** was prepared (83.7 mg, 69 %) according to GP II (EA / HX, 2:1) 5-bromo-3-(4-methoxyphenyl)-1H-pyrrolo[2,3-b]pyridine (117 mg, 0.39 mmol) and 3-aminophenylboronic acid (71.8 mg, 0.46 mmol) as white solid. mp 209 – 210 °C. ¹H NMR (400 MHz, DMSO-*d*₆) δ 11.84 (s, 1H), 8.45 (d, *J* = 1.8 Hz, 1H), 8.26 (d, *J* = 2.1 Hz, 1H), 7.76 (d, *J* = 2.4 Hz, 1H), 7.66 (d, *J* = 8.7 Hz, 2H), 7.12 (t, *J* = 7.7 Hz, 1H), 7.02 (d, *J* = 8.7 Hz, 2H), 6.90 (s, 1H), 6.85 (d, *J* = 7.6 Hz, 1H), 6.57 (dd, *J* = 8.1, 2.3 Hz, 1H), 5.15 (s, 2H), 3.78 (s, 3H). ¹³C NMR (100 MHz, DMSO-*d*₆) δ 157.54, 149.14, 148.42, 141.63, 139.64, 129.44, 129.39, 127.58, 127.42, 124.79, 123.47, 117.28, 114.65, 114.38, 112.67, 112.43, 55.07. HRMS (EI+) *m/z* calcd for C₂₀H₁₇N₃O [M + H]⁺, 316.1450; found 316.1424.

3-(3,4-dimethoxyphenyl)-5-(pyridin-4-yl)-1H-pyrrolo[2,3-b]pyridine (24). Compound **24** was prepared (19.9 mg, 72%) according to GP II (CH₂Cl₂ / MeOH, gradient 30:1 to 10:1) from 5-bromo-3-(3,4-dimethoxyphenyl)-1H-pyrrolo[2,3-b]pyridine (28 mg, 0.084 mmol) and 4-pyridinylboronic acid (12.4 mg, 0.101 mmol) as white solid. mp 218 – 220 °C. ¹H NMR (400 MHz, Chloroform-*d*) δ 10.01 (s, 1H), 8.72–8.65 (m, 3H), 8.40 (d, *J* = 2.0 Hz, 1H), 7.57 (d, *J* = 5.5 Hz, 2H), 7.52 (d, *J* = 2.2 Hz, 1H), 7.20 (dd, *J* = 8.3, 2.0 Hz, 1H), 7.12 (d, *J* = 2.0 Hz, 1H), 7.00 (d, *J* = 8.2 Hz, 1H), 3.95 (s, 3H), 3.94 (s, 3H). ¹³C NMR (100 MHz, DMSO-*d*₆) δ 150.09, 149.27, 149.17, 147.38, 146.11, 141.75, 127.45, 125.74, 125.41, 124.36, 121.41, 118.79, 117.44, 115.20,

112.47, 110.72, 55.60. HRMS (EI+) m/z calcd for $C_{20}H_{17}N_3O_2$ [M + H]⁺, 332.1399; found 332.1372

3-(3-(pyridin-3-yl)-1H-pyrrolo[2,3-b]pyridin-5-yl)aniline (25).

5-bromo-3-(pyridin-3-yl)-1H-pyrrolo[2,3-b]pyridine was

prepared (38.5 mg, 65%) according to GP I (EA / HX, gradient 1:1 to 3:1) from 5-bromo-3-iodo-1-(phenyl-sulfonyl)-1H-pyrrolo[2,3-b]pyridine (100 mg, 0.216 mmol) and 3-pyridinyl boronic acid (32 mg, 0.26 mmol). ¹H NMR (300 MHz, CD₃OD-*d*₄) δ 8.78 (dd, *J* = 0.75, 2.2 Hz, 1H), 8.39 (dd, *J* = 1.6, 4.9 Hz, 1H), 8.36 (d, *J* = 2.1 Hz, 1H), 8.28 (d, *J* = 2.1 Hz, 1H), 8.05–8.09 (m, 1H), 7.80 (s, 1H), 7.46 (dd, *J* = 4.9, 7.2 Hz, 1H). Compound **25** was prepared (17.7 mg, 22%) according to GP II (CH₂Cl₂ / MeOH, gradient 20:1 to 10:1) from 5-bromo-3-(pyridin-3-yl)-1H-pyrrolo[2,3-b]pyridine (76 mg, 0.28 mmol) and 3-aminophenylboronic acid (52 mg, 0.336 mmol) as gray solid. mp 225 – 227 °C. ¹H NMR (400 MHz, DMSO-*d*₆) δ 12.13 (s, 1H), 9.00 (d, *J* = 2.3 Hz, 1H), 8.50 (d, *J* = 2.0 Hz, 1H), 8.46 (dd, *J* = 4.8, 1.6 Hz, 1H), 8.34 (d, *J* = 2.1 Hz, 1H), 8.17 (dt, *J* = 7.8, 2.0 Hz, 1H), 8.05 (s, 1H), 7.46 (dd, *J* = 7.9, 4.7 Hz, 1H), 7.12 (t, *J* = 7.8 Hz, 1H), 6.93 (s, 1H), 6.89 (d, *J* = 7.6 Hz, 1H), 6.57 (dd, *J* = 9.0, 1.7 Hz, 1H), 5.17 (s, 2H). ¹³C NMR (100 MHz, DMSO-*d*₆) δ 149.16, 148.52, 147.21, 146.64, 142.08, 139.41, 133.35, 130.90, 129.86, 129.46, 125.28, 124.88, 123.93, 117.09, 114.74, 112.78, 112.49, 111.10. HRMS (EI+) m/z calcd for $C_{18}H_{14}N_4$ [M + Na]⁺, 309.1116; found, 309.1117.

4-(3-(3,4-dimethoxyphenyl)-1H-pyrrolo[2,3-b]pyridin-5-yl)aniline (26).

Compound **26** was prepared (29.3 mg, 57%) according to GP II (EA / HX, gradient 1:1 to 3:1) from 5-bromo-3-(3,4-dimethoxyphenyl)-1H-pyrrolo[2,3-b]pyridine (50 mg, 0.15 mmol) and 4-(4,4,5,5-tetramethyl-1,3,2-dioxaborolan-2-yl)aniline (39.5 mg, 0.18 mmol) as yellow solid. mp 203 – 205 °C. ¹H NMR (400 MHz, DMSO-*d*₆) δ 11.76 (d, *J* = 2.7 Hz, 1H), 8.44 (d, *J* = 2.1 Hz, 1H), 8.23 (dd, *J* = 2.1, 0.6 Hz, 1H), 7.77 (d, *J* = 2.6 Hz, 1H), 7.41 (d, *J* = 8.5 Hz, 2H), 7.28 (dd, *J* = 8.1, 2.1 Hz, 1H), 7.25 (d, *J* = 2.0 Hz, 1H), 7.02 (d, *J* = 8.2 Hz, 1H), 6.68 (d, *J* = 8.5 Hz, 2H), 5.16 (s, 2H), 3.85 (s, 3H), 3.78 (s, 3H). ¹³C NMR (100 MHz, DMSO-*d*₆) δ 149.15, 147.91, 147.87, 147.18, 141.26, 129.35, 128.02, 127.52, 126.41, 123.79, 123.51, 118.56, 117.40, 114.49, 114.43, 112.49, 110.58, 55.59, 55.58. HRMS (EI+) m/z calcd for $C_{21}H_{19}N_3O_2$ [M + H]⁺, 346.1556; found 346.1534.

Acknowledgements

This research was supported by National Research Foundation of Korea (NRF) through general research grants NRF-2011-0022858, 0016436, 0020322) and the Institute for Basic Science (IBS).

Notes and references

[§]Department of Bioscience and Biotechnology, Sejong University, Seoul 143-747, Korea. Fax: (+82) 2-3408-3766; Tel: (+82) 2-3408-2811; E-mail: hspark@sejong.ac.kr

[§]Department of Chemistry, Korea Advanced Institute of Science and Technology (KAIST), Daejeon, 305-701, Korea. Fax: (+82) 42-350-2810; Tel: (+82) 42-350-2811; E-mail: hongorg@kaist.ac.kr

† Electronic Supplementary Information (ESI) available: See DOI: 10.1039/b000000x/

1. a) R. Roskoski, *Bioch. Biophys. Res. Commun.* **2005**, 338, 1307; b) T. Hunter, *Cell* **1995**, 80, 225.

2. a) L. K. Ashman, R. Griffith, *Expert Opin. Investig. Drugs* **2013**, 22, 103; b) J. Lennartsson, L. Rönstrand, *Physiol. Rev.* **2012**, 92, 1619.
3. J. Lennartsson, T. Jelacic, D. Linnekin, R. Shivakrupa, *Stem Cells* **2005**, 23, 16.
4. a) S. Forbes, J. Clements, E. Dawson, S. Bamford, T. Webb, A. Dogan, A. Flanagan, J. Teague, R. Wooster, P. A. Futreal, M. R. Stratton, *Br. J. Cancer* **2006**, 94, 318; b) A. Maleddu, M. A. Pantaleo, M. Nannini, B. M. Di, M. Saponara, C. Lolli, G. Biasco, *Oncol. Rep.* **2009**, 21, 1359.
5. R. J. Chian, S. Young, A. Danilkovitch-Miagkova, L. Ronnstrand, E. Leonard, P. Ferrao, L. Ashman, D. Linnekin, *Blood* **2001**, 98, 1365.
6. H. Bougherara, F. Subra, R. Crepin, P. Tauc, C. Auclair, M. A. Poul, *Mol. Cancer Res.* **2009**, 7, 1525.
7. a) E. Laine, I. C. de Beauchene, D. Perahia, C. Auclair, L. Tchertanov, *PLoS Comput. Biol.* **2011**, 7, e1002068; b) Y. L. Lin, B. Roux, *J. Am. Chem. Soc.* **2013**, 135, 14741; c) D. Thompson, C. Miller, F. O. McCarthy, *Biochemistry*, **2008**, 47, 10333; d) N. Kansal, O. Silakari, M. Ravikumar, *Eur. J. Med. Chem.* **2010**, 45, 393; e) C. D. Mol, K. B. Lim, V. Sridhar, H. Zou, E. Y. T. Chien, B. C. Sang, J. Nowakowski, D. B. Kassel, C. N. Cronin, D. E. McRee, *J. Biol. Chem.* **2003**, 278, 31461; f) M. Torrent, K. Rickert, B. S. Pan, L. Sepp-Lorenzino, *J. Mol. Graph. Model.* **2004**, 23, 153.
8. a) M. J. Frost, P. T. Ferrao, T. P. Hughes, L. K. Ashman, *Mol. Cancer Ther.* **2002**, 1, 1115; b) Y. Ma, S. Zeng, D. D. Metcalfe, C. Akin, S. Dimitrijevic, J. H. Butterfield, G. McMahon, B. J. Longley, *Blood* **2002**, 99, 1741; c) K. S. Gajiwala, J. C. Wu, J. Christensen, G. D. Deshmukh, W. Diehl, J. P. DiNitto, J. M. English, M. J. Greig, Y. A. He, S. L. Jacques, E. A. Lunney, M. McTigue, D. Molina, T. Quenzer, P. A. Wells, X. Yu, Y. Zhang, A. Zou, M. R. Emmett, A. G. Marshall, H. M. Zhang, G. D. Demetri, *Proc. Natl. Acad. Sci. USA* **2009**, 106, 1542; d) G. D. Demetri, M. von Mehren, C. D. Blanke, A. D. van den Abbeele, B. Eisenberg, P. J. Roberts, M. C. Heinrich, D. A. Tuveson, S. Singer, M. Janicek, J. A. Fletcher, S. G. Silverman, S. L. Silberman, R. Capdeville, B. Kiese, B. Peng, S. Dimitrijevic, B. J. Druker, C. Corless, C. D. Fletcher, H. Joensuu, *N. Engl. J. Med.* **2002**, 347, 472.
9. A. S. Corbin, S. Demehri, I. J. Griswold, Y. Wang, C. A. Metcalf III, R. Sundaramoorthi, W. C. Shakespeare, J. Snodgrass, S. Wardwell, D. Dalgarno, J. Iulucci, T. K. Sawyer, M. C. Heinrich, B. J. Druker, M. W. Deininger, *Blood* **2005**, 106, 227.
10. C. Zhang, P. N. Ibrahim, J. Zhang, E. A. Burton, G. Habets, Y. Zhang, B. Powell, B. L. West, B. Matusow, G. Tsang, R. Shellooe, H. Carias, H. Nguyen, A. Marimuthu, K. Y. Zhang, A. Oh, R. Bremer, C. R. Hurt, D. R. Artis, G. Wu, M. Nespi, W. Spevak, P. Lin, K. Nolop, P. Hirth, G. H. Tesch, G. Bollag, *Proc. Natl. Acad. Sci. USA* **2013**, 110, 5689.
11. B. K. Shoichet, A. R. Leach, I. D. Kuntz, *Proteins* **1999**, 34, 4.
12. C. D. Mol, K. B. Lim, V. Sridhar, H. Zou, E. Y. Chien, B. C. Sang, J. Nowakowski, D. B. Kassel, C. N. Cronin, D. E. McRee, *J. Biol. Chem.* **2003**, 278, 31461.
13. A. Sali, T. L. Blundell, *J. Mol. Biol.* **1993**, 234, 779.
14. C. D. Mol, D. R. Dougan, T. R. Schneider, R. J. Skene, M. L. Kraus, D. N. Scheibe, G. P. Snell, H. Zou, B. C. Sang, K. P. Wilson, *J. Biol. Chem.* **2004**, 279, 31655.
15. B. Nolen, S. Taylor, G. Ghosh, *Mol. Cell* **2004**, 15, 661.
16. J. Vendôme, S. Letard, F. Martin, F. Svinarchuk, P. Dubreuil, C. Auclair, M. Le Bret, *J. Med. Chem.* **2005**, 48, 6194.
17. See the Supporting Information for more details.
18. a) R. Wang, Y. Gao, L. Lai, *J. Mol. Model.* **2000**, 6, 498; b) T. Rodrigues, F. Roudnicki, C. P. Koch, T. Kudoh, D. Reker, M. Detmara, G. Schneider, *Chem. Sci.* **2013**, 4, 1229; c) G. Schneider, *J. Comput.-Aided Mol. Des.*, **2012**, 26, 115; d) K. Hasegawa, M. Keiya, K. Funatsu, *Mol. Inf.*, **2010**, 29, 793.
19. a) S. Hong, S. Lee, B. Kim, H. Lee, S.-S. Hong, S. Hong, *Bioorg. Med. Chem. Lett.* **2010**, 20, 7212; b) S. Gourdain, J. Dairou, C. Denhez, C. L. C. Bui, F. Rodrigues-Lima, N. Janel, J. M. Delabar, K. Cariou, R. H. Dodd, *J. Med. Chem.*, **2013**, 56, 9569.
20. The IC₅₀ determinations were performed at the Reaction Biology Corp (Malvern, PA, USA). See the Supporting Information for more details.